Thevenin Impedance Concept for Fast Detection of Microgrid Islanding Scenarios in the Presence of Small Synchronous Generators

I. Sepehrirad[1], R. Ebrahimi[1,], E. Alibeiki[2], S. Ranjbar[3]*

[1] *Department of Electrical Engineering, Gorgan Branch, Islamic Azad University, Gorgan, Iran*
[2] *Department of Electrical Engineering, Aliabad Katoul Branch, Islamic Azad University, Aliabad Katoul, Iran*
[3] *Department of electrical engineering, Velayat University, Iranshahr, Iran*

Abstract— *Modern power systems deal with different stability concerns due to operation near to their critical margins. Implementing the small energy resources and online islanding schemes perform as a modification scheme for increasing the system overall stability. This paper presents an adaptive approach for online detection of islanding microgirds in the presence of renewable energy resources consisting of diesel generators. For this issue, based on the concept of thevenin impedance, the microgrid impedance matrix is evaluated. In this case, considering the system angular frequency as an online index within different operating conditions, the islanding operating cases are identified. The proposed scheme uses an online non-model-based index which provides high impedance values in the case of grid-connected operating mode. Through continuous time window, the system impedance derivatives-based matrix is provided which islanding operating scenarios are estimated. In this case, considering a set of analytical evaluations, the required adaptive parameters and corresponding online adjustments are provided.*

The proposed approach is carried out through a modified microgrid test system consisting of synchronous generators which considering different cases studies, the proposed scheme ability is evaluated. It is revealed that through different case studies about 100 ms time duration is required to estimate an islanding operating condition which the proposed MICI index goes lower than criteria. Simulation results dedicate the effectiveness of the proposed approach for online and fast identification of islanding scenarios with respect to other corresponding techniques.

Keywords—Islanding identification, Microgrid, Synchronous generators, Thevenin impedance matrix.

NOMENCLATURE

Abbreviations

AVR	Automoatic Voltage Requlator
CCP	Common Coupling Pojnt
DG	Distributed Generator
DT	Decision Tree
GCOM	Grid Connected Operating Point
IBSR	Inverter-Based Static Resources
IOM	Islanded Operating Mode
MG	Microgrid
MICI	Microgrid Islanding Condition Index
NDZs	Non-Detection Zones
RES	Renewable Energy Resources
ROCOR	Rate of Change of Resistance
SLD	Single Line Diagram
SSG	Small Synchronous Generators

Variables

δ	Generator rotor angle
Δt	Time windows
ΔP_e	Microgrid active power exchanged from DG to upstream network
$\Delta \omega$	System frequency oscillation
Δa	Small deviations
ΔP_m	Microgrid mechanical power exchanged from DG to upstream network
a	The load parameter
b	Load parameter
D	Damping coefficient
$d\delta$	Rotor angle deviation
E_G	Synchronous generators internal voltage
E_{THG}	System Thevenin voltage
H	Inertia coefficient
I_G	SSG output current.
R_G	Resistance impedances seen from generator terminals
V_G	SSG output voltage
X_G	Reactance impedances seen from generator terminals
X_{intG}	Synchronous generators internal reactance
X_{TH-sys}	Upstream equivalent impedance
X_{THG}	Thevenin impedance seen from generator terminals
X_{Tr-G}	Transformer impedance connected to generator buses
Z_{DL}	Load impedance
E_G	Voltage source
I_{diff}	Differential current I_{diff} at each time step
k_1	Static constant value
k_f	Load coefficient depends on the microgrid frequency
P_0	Load initial active power
P_L	Load active power
Q_0	Load initial reactive power
Q_L	Load reactive power

R_0 Total microgrid load resistance
$R_{G(GCOM)}$ Equivalent resistance evaluated from generator bus in grid-connected mode
$R_{G(IM)}$ Equivalent thevenin resistance in islanded mode
R_L Load resistance
V_0 Nominal voltage ratio
$X_{G(GCOM)}$ Equivalent reactance evaluated from generator bus in grid-connected mode
X_L Load reactance
Z_{GT} Equivalent generator terminals impedance
Z_G Equaled impedance

1. INTRODUCTION

Increasing power demands through today's distribution systems resulted in the system are operated near to theirs critical margins. In this case, implementing small scale energy resources as small synchronous generators (SSG) are performed as a modification scheme for increasing the overall system reliability.

1.1. Paper Motivation

Depending on the system topologies and restructures, distributed system can be operated through two different grid-connected operating mode (GCOM) and islanded operating modes (IOM). In the case of islanded mode which is known as microgrid (MG) system, by using a set of SSGs located at different buses, it is possible to supply system demands and provide overall system security. However, because of the SSG capability levels, it is not possible to operate them through all of GCOM and IOM conditions. Therefore, identifying the IOM situations and evaluating corresponding SSG requirements are revealed as the most important issues through microgrid operating conditions [1]. In this case, there are one or more SSGs which are responsible to supply a set critical loads [2]. Accurate estimations and speed ratios of the equipment are two main issues which is in the case of failure scenarios with respect to each provided issues, MGs are involved within different problems as system securities, protection failures, consecutive occurrences to installed SSGs where in the case of sever conditions, it maybe resulted in cascading failures and corresponding microgird blackouts [1].

1.2. Literature Review

The IEEE committee develops some useful standards for microgrid proper operations where the standard 1547 comments that an islanding operating scenario must be identified lower than 2 seconds in all of load level conditions. In order to meet with the provided requirements, there are different approaches presented by power engineers which can be developed through two different local signal-based and global signal-based schemes [3]. Considering cost constraints, the methods based on local approaches are more favorite by engineers through recent provided schemes. However, the global signal-based approaches have own considerable advantages where in the case of failing islanding identification techniques, by ignoring the system non-detection zones (NDZs), the system load flow imbalances are evaluated which the required SSGs are estimated [4].

In the case of local signal-based approach, the provided techniques are categorized through two active and passive schemes. In this case, the active-based schemes are related to evaluate SSG voltage and frequency controllers with respect to some noise signals combined with corresponding controller's input signals. Most of the corresponding active schemes can be provided as sandia-based frequency and voltage technique [5, 6], drift mode method [7], evaluating the negative sequence of current signals through voltage and frequency controllers [8] and frequency shift technique considering slip mode evaluations [9]. Also, there are some global-based schemes which are concentrated to decrease NDZ locations [10] which involve with some power system

stability and corresponding power quality issues. The evaluated results through developed controlling approaches show that they have provided proper results when some inverter-based sources with low zero inertia values are connected through microgrid system. In the case of some synchronous generators are used as MG main resources, the provided schemes are not able to provide proper controlling behavior through different operating conditions.

For solving this issue, in other cases, there are other controlling schemes called as passive approaches which are concentrated to control rotational machine resources as synchronous generators in the case of islanded operating modes. There are different methods within passive-based approaches which are concentrated through under/over voltage and under/over frequency controls [11] and rate of change of frequency (ROCOF) with respect to voltage phase shift ratio [12]. In this case, [13, 14] develop some similar schemes considering individual NDZ matrixes through large scale MG systems. In order to resolve the NDZ issue, by evaluating frequency deviations of synchronous generators through time domain and identifying the corresponding damping ratios, [3] and [15, 16] present some passive techniques to control the SSG frequencies and voltages. However, through these references, it is considered that the islanded microgrid system frequency is deviated through smooth behaviors which there are no frequency oscillations through frequency deviations. Also, in the case of GCOM, because of the large-scale system connected to microgrid, there are frequency oscillations which the MG's frequency is oscillated with respect to installed synchronous generators inertias and provided fault events. It should be noted that both of oscillation and non-oscillation scenarios are applicable with corresponding individual discussions. In the case of SSGs equipped with individual governors, depending on the governor responses, microgrid presents different frequency oscillations [15]. If, there are improper synchronization torques into the system, SSGs provide some unstable frequency behaviors which depends on the loss of required torque value, different frequency oscillations are provided in the microgrids [17]. For this issue, [18] presents a passive controlling scheme in microgrid IOM which works based on the frequency deviation ratio through time domain evaluations for providing required reactive power values. In this case, the mentioned transient and steady state frequency stability thresholds are identified through various simulation case studies.

Also, there are some non-model-based techniques which use some data mining techniques as fuzzy logic [19] for identifying an islanding operating scenario through real-time fault event scenarios. Similarly, [20] presents a decision tree-based (DT) data mining technique for online detection of SSG-based MG islanding scenarios which develops the system reactance distributed through multiple harmonic orders as the DT input features. In this case, the main objective function and corresponding controller accuracies are highly depends on the expansion of the training data. In the case of intelligent algorithm do not trained properly within all of possible fault events, the algorithm output estimations are inaccurate which maybe resulted in incorrect decisions for online identification of islanding scenarios.

1.3. Paper Contributions

In this paper, an adaptive global signal-based passive controlling scheme is proposed for online islanding identification of microgrids consisting of small-scale synchronous generators. For this issue, based on the thevenin impedance concept achieved from generator terminal buses, the equivalent impedance matrix of MG is provided from which the system voltage and frequency constraints are controlled. In this case, considering a set centralized loads dependence on the system voltage and frequency and providing them through mathematical formulations the corresponding proposed adaptive controller is provided. The proposed algorithm is an online and model-based scheme which provides small scale of DNZ matrixes resulted in fast and accurate

estimations between islanding and other fault event scenarios which can be implemented properly through microgrid protection strategies.

1.4. Paper Organizations

This paper is organized as follows. Considering developed algorithm, Section 2 provides the conceptual structure of the proposed scheme through specific indexes for accurate estimation of islanding operating modes. According to provided structure, Section 3 develops the required analytical discussions and thresholds through mathematical formulations. Based on the provided descriptions, different simulation case studies are investigated in Section 4 which the effectiveness of the proposed scheme under various voltage and frequency protecting conditions are evaluated. Finally, conclusions and discussions are provided in Section 5.

2. CONCEPTUAL STRUCTURE OF THE PROPOSED ISLANDING IDENTIFICATION SCHEME

This section develops the conceptual structure of the proposed scheme through microgrid systems are equipped with synchronous generator resources. To do this, considering proposed approach methodology, the corresponding structures are detailed through different subsection as follows.

2.1. Mathematical Description of Microgrid Operating Modes

In this section, considering a small scale microgrid consisting of SSGs resources and different loads dependence on the system voltage and frequency, the basic concept of proposed index for online identification of islanding cases is developed. Single line diagram (SLD) of the mentioned microgrids consisting of SSGs and corresponding load buses is illustrated in Fig. 1.

From Fig. 1, considering a common coupling point (CCP), microgrid can be connected to upstream networks and operated through grid-connected operating mode. In the case of GCOM, the output voltages of generator buses are provided as follows [5]:

$$V_G = E_G \llcorner \delta - j X_{intG} I_G \qquad (1)$$

Where, E_G and X_{intG} are the synchronous generators internal voltage and reactance, respectively. Also, V_G and I_G represent the SSG output voltage and current, respectively.

Considering SSG's voltage and current parameters as (1), the corresponding complex impedance seen from generator terminals in GCOM ($Z_{GT-GCOM}$) is resulted as follows [5]:

$$Z_{GT(GCOM)} = V_G / I_G = [E_G \llcorner \delta / I_G] - j[X_{intG}] \qquad (2)$$

Where, R_G and X_G are the resistance and reactance impedances seen from generator terminals.

In the case of GCOM, considering the upstream equivalent impedance as X_{TH-sys}, dependence load impedance as Z_{DL} and transformer impedance connected to generator buses as X_{Tr-G}, the corresponding equivalent Thevenin impedance seen from generator terminals (X_{THG}) can be evaluated as follows [5]:

$$Z_{THG} \cong X_{THG} = (Z_{DL}||X_{TH-sys}) + X_{Tr-G} \qquad (3)$$

Into the microgrids operating conditions, the systems elements are connected together with small line impedances. In Figure 2, however, the line is presented into the system model, but comparing with other impedances values, it is neglected into the mathematical formulation.

From (3), according to small effects of equivalent Thevenin resistance, it is ignored through final equivalent impedance evaluation. Considering the system Thevenin voltage as E_{THG}, final model of the microgrid equivalent circuit simplified through

Thevenin equivalent model can be represented as simplified SLD model showed in Fig. 2.

From Fig. 2, the generator output current I_G is evaluated as follows [5]:

$$I_G = (E_G \llcorner \delta - E_{TH-sys} \llcorner 0)/j(X_{intG} + X_{THG}) \qquad (4)$$

Replacing (4) in (2), the equivalent generator terminals impedance Z_{GT} is calculated as follows

$$Z_{GT(GCOM)} = \left[\underbrace{\frac{E_G \angle \delta}{(E_G \angle \delta - E_{TH-sys} \angle 0)} \times j\left(X_{intG} + X_{THG}\right)}_{R_G} \right]$$
$$- j \underbrace{[X_{intG}]}_{X_G} \qquad (5)$$

From (5), by considering $\alpha = (E_{TH-sys}/E_G)$ and assuming some simplifications, the corresponding equivalent reactance $X_{G(GCOM)}$ and resistance $R_{G(GCOM)}$ evaluated from generator bus in grid-connected mode can be presented as follows [5]:

$$R_{G(GCOM)} = \frac{\alpha \times \sin \delta}{(1 + \alpha^2 - 2\alpha \times \cos \delta)} \times (X_{intG} + X_{THG}) \qquad (6)$$

$$X_{G(GCOM)} = \left[\frac{1 - \alpha \times \cos \delta}{(1 + \alpha^2 - 2\alpha \times \cos \delta)} \times (X_{intG} + X_{THG}) \right] - X_{intG} \qquad (7)$$

According to (6) and (7), the generator real and image impedances are depended in the generator rotor angle δ where in the case of fault occurrence resulted in angle deviations, the evaluated generator impedances R_G and X_G are oscillated, correspondingly.

In another case, by opening the CCP circuit breaker in Fig. 1, microgrid is disconnected from the upstream network which is operated through islanded operating mode. Considering similar mathematical formulations, it is possible to present microgrid Thevenin model. Fig. 3 presents the microgrid SLD in islanded operating mode simplified through Thevenin equivalent model. From Fig. 3, the equivalent Thevenin resistance ($R_{G(IM)}$) and reactance impedances evaluated from generator terminals in islanded operating mode are calculated as follows [5]:

$$Z_{GT(IM)} = Z_{DL} + jX_{Tr-G} = R_{G(IM)} + jX_{G(IM)} \qquad (8)$$

In the case of ignoring the load dependencies on the system voltage and frequency, result of resistance derivative with respect to rotor angle deviations ($dR_G/d\delta$) goes to zero value which means there are a set of constant impedance loads installed into microgrid system. In some special cases, derivative results are not equaled with zero values. Reasons of this situations will be discussed in Section 3. Based on the derivative results of the equivalent resistance with respect to rotor angle deviations ($dR_G/d\delta$), it can be used an adaptive index as rate of change of resistance (ROCOR) index for online identification of islanded modes from other fault event scenarios. In this case, considering equivalent resistance R_G presented in (6), adaptive ROCOR index is presented as follows [13]:

$$ROCOR = \frac{dR_G}{d\delta} = -\frac{2\alpha^2 - \alpha \cos \delta(\alpha^2 + 1)}{(1 + \alpha^2 - 2\alpha \times \cos \delta)^2}$$
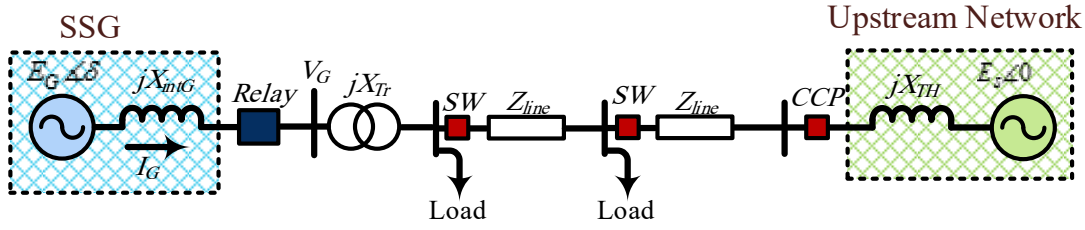$$\times (X_{intG} + X_{THG}) \qquad (9)$$

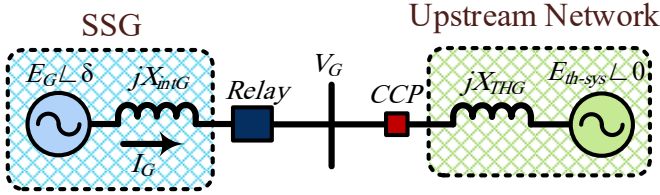Fig. 1. Single line diagram of microgrid consisting of SSGs and dependence loads [5]

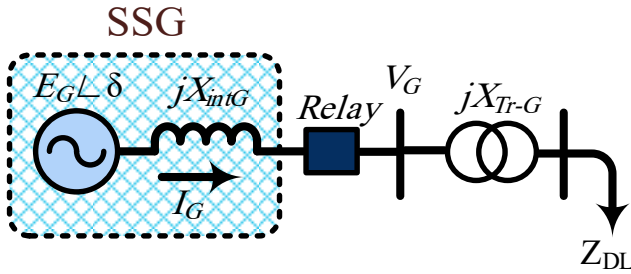Fig. 2. Microgrid Thevenin equivalent circuit through grid-connected operating mode [5]

Fig. 3. Microgrid Thevenin equivalent circuit through islanded operating mode [5].

In real power systems, there are several synchronous generators and power transformers which are operated together in high voltage values. In this case, based on the system operating levels in high voltage ratios, the value of resistance is about 0.1 or lower than system reactance value which considering some simplifications, it can be ignored through the synchronous generators/power transformer model. In this case, each power systems are modelled with several types reactance which are related to the generators, transformers or transmission lines. In another case through lower voltage levels as operated into the microgrid/distributed networks, the system resistance values are close or higher than the system reactance which they cannot be ignored into the system model. In this case, the effects of resistance values are much higher than reactance value which known as an important index for evaluating the system security conditions. Therefore, in this paper, in the case of modelling power system and power transformer, by ignoring the power system resistances, only system reactances are considered into the system model. While into the microgrid voltage level, both microgrid resistance and reactance values are modelled which the resistance type is used through the proposed ROCOR identification scheme.

In this case, at each time windows Δt, considering a fault event scenario, the corresponding generator rotor angles can be represented as follows [13]:

$$\delta_{t+1} = \delta_t + \Delta\delta \tag{10}$$

$$\Delta\delta = t \times \Delta\omega \tag{11}$$

Where, δ_{t+1}, δ_t and $\Delta\delta$ are rotor angles measurements through Δt evaluations. Also, $\Delta\omega$ represents the system frequency oscillation with respect to fault event scenario.

From (10) and (11), it can be revealed that depending on the system frequency deviations $\Delta\omega$, generator rotor angles are deviated which means a direct relationship through δ and ω. In the case of constant ω values (i.e. $\Delta\omega = 0$), it can be neglected rotor angle deviations $\Delta\delta$ through time domain evaluations. Considering provided descriptions, the proposed adaptive index (9) can be extended through $\Delta\omega$ deviations as follows [13]:

$$ROCOR = \frac{dR_G}{d\omega} = -\frac{2\alpha^2 - \alpha\cos\delta(\alpha^2 + 1)}{(1 + \alpha^2 - 2\alpha \times \cos\delta)^2} \\ \times (X_{intG} + X_{THG}) \times t \tag{12}$$

From (12), it is concluded that when $\alpha = (E_{TH-sys}/E_G)$ goes to zero ($\alpha = 0$) (i.e. microgrid is disconnected from upstream network), the corresponding ROCOR index will be equaled to zero which means an islanding operating mode has been occurred. On the other hand, at each time windows Δt, based on the online measuring devices installed in the system, the proposed index ROCOR is measured and evaluated. In the case of ROCOR is evaluated greater than zero (i.e. ROCOR>0.005), it means a GCOM which microgird is operated through grid-connected mode. However, in the case of ROCOR is evaluated through tiny values (ROCOR<0.005), means IOM condition which microgird is operated through islanded operating mode.

It is worth noting that, the threshold value of 0.005 is a security threshold criterion achieved based on try and error evaluations which individually used in this paper.

As it can be seen, it is revealed that the proposed adaptive index can estimates the IOM scenarios properly with respect to other fault event scenarios. Considering developed scheme, there are some individual thresholds must be specified with respect to each microgrid system which are discussed through Section 3. In (12), the required frequency deviation $\Delta\omega$ can be evaluated through either indirect or direct-based methods. Considering direct schemes, there are some speed sensors which are responsible to evaluate

the generators rotor speed. However, through indirect-based schemes, by using synchronous generator differential equations, the system frequency deviation is calculated. Details descriptions related to direct and indirect-based method can be found in [21-22].

It is worth noting that when both synchronous generator and inverter-based static resources (IBSR) are used through microgrid operation conditions, the system frequency is oscillated through islanding condition which is involved with different power flow imbalances through islanded mode. In this case, the equivalent resistance R_G deviations are highly depends on the system load type and corresponding dependencies. Therefore, the proposed scheme is an adaptive index which can be used through both SSG and hybrid resources.

2.2. Detailed Structure of the Proposed Identification Index

As it is explained in Section 2.1, in the case of static impedance load models, the proposed *ROCOR* index goes to zero with respect to all islanded operating modes. Also, real-time evaluations showed that dependency of resistance load models are much lower than voltage dependency cases which there are low sensitivities with respect to constrained frequency deviations (e.g. $\Delta f = \pm 0.5$ Hz). Therefore, by considering some simplifications, the loads frequency dependency can be ignored from which only voltage dependency is considered through load models. In this case, the loads dependency models are presented as follows [13]:

$$P_L = P_0 \left(\frac{V_{LF}}{V_0} \right)^a \qquad (13)$$

$$Q_L = Q_0 \left(\frac{V_{LF}}{V_0} \right)^b \qquad (14)$$

where, P_0, Q_0, P_L and Q_L are the loads active and reactive powers with respect to initial and rated values, respectively. V_{LF} and V_0 represent the initial and load flow voltages.

Also, a and b represent two individual coefficients between $a = b = 0$ to $a = b = 2$ values which are specified with respect to load models. In the case of modelling load parameters considering two equations (13) and (14), dynamic behaviors are modeled. In this case, there are three types of loads as constant impedance ($a = 2, b = 2$), constant current ($a = 1, b == 1$) and constant power ($a = 0, b = 0$) specified by a and b parameters developed in (13) and (14). It should be noted that the parameters a and b are performed with respect to system load level. Considering load types, the parameter a and b are changed from which in the case of individual loads, it is estimated about 0 to 2 values. However, in the case of developing composite load models, considering parameters within 0.5 to 1.8, the load diversity factors are provided [17].

It should be noted that the corresponding frequency dependency is investigated through required threshold constraints which are detailed in Section 3. Also, it is worth noting that, however, the proposed ROCOR index

has been developed through static load models, real-time evaluations revealed that it presents proper results through rotational load models as induction machines and so on. In (14), considering $k_1 = (V_0)^a / P_0$ and $k_2 = (V_0)^b / Q_0$, the corresponding load resistance R_L and reactance X_L can be written as follows [13]:

$$k_1 = R_L / (V_{LF})^{2-a} \qquad (15)$$

$$k_2 = X_L / (V_{LF})^{2-b} \qquad (16)$$

In (15), k_1 represents a static constant value which its derivative function with respect to SSG speed deviation ($dk_1/d\omega$) will be equaled to zero value. In the case of IOM, the equivalent resistant R_G seen from generator terminals is equaled to load resistance R_L which the corresponding derivative function (15) with respect to system frequency ($dk_1/d\omega$) is resulted in zero value as follows:

$$\frac{dk_1}{d\omega} = \left(\frac{d\left(R_L / (V_{LF})^{2-a} \right)}{d\omega} \right) \cong \left(\frac{d\left(R_G / (V_{LF})^{2-a} \right)}{d\omega} \right) \cong 0 \qquad (17)$$

It should be noted that, in the case of GCOM, the equivalent resistance R_G is not equaled with load resistance R_L (i.e. $R_G \neq R_L$) which is resulted in nonzero values for derivative function (17). As a result, based on (12), the corresponding Thevenin resistance R_G is a function of rotor angle deviations $d\delta$ which in the case of SSG sources installed in microgrid, the corresponding derivative function (17) is resulted in nonzero values. Therefore, considering resistance behaviors with respect to system frequency, the corresponding microgrid islanding condition index (MICI) is presented as follows:

$$MICI = \left(\frac{(V_0)^{2-a}}{R_0} \right) \times \left| \left(\frac{d\left(R_G / (V_{LF})^{2-a} \right)}{d\omega} \right) \right| \qquad (18)$$

Where, R_0 represents the total microgrid load resistance operated through nominal voltage ratio V_0.

As a result, the proposed ROCOR index is proper for static load models. However, in the case of dynamic load models, it is better to use the proposed MICI index through real-time evaluations.

In (18), the parameters $[(V_0)^{2-a}/R_0]$ is performed to normalize the proposed index with respect to system load level. In order to investigate all of complicate load models, considering parameter a between two minimum $a_{\min} = 0$ and maximum $a_{\max} = 2$ thresholds, the identification performance of proposed *MICI* index is evaluated. In this case, there are different *MICI* indexes provided through a parameters which the lowest value of *MICI* index is determined as final ratio as follows:

$$MICI_{\min} = \min \left[MICI_1(a_1), MICI_2(a_2), \ldots, MICI_i(a_i) \right.$$
$$\left. , \ldots, MICI_n(a_n) \right] \qquad (19)$$

Where, i and n represent the parameter a numbers through different values resulted in different accuracy ratio.

Considering each individual a_i through (18), the $MICI_i$ index with corresponding precision ratio is provided. Also, in the case of dynamic load models, depending on the fault event scenario, loads parameters are varied which
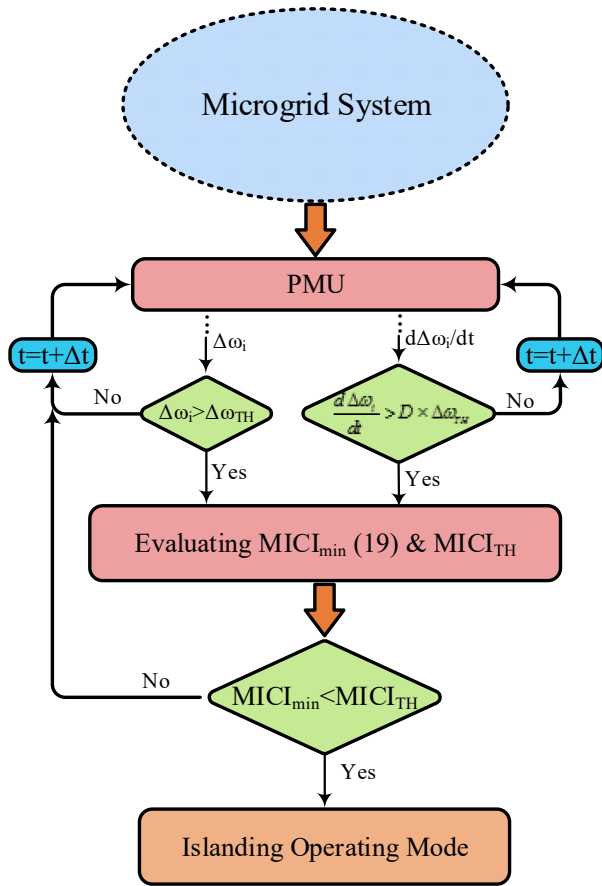
Fig. 4. Real-time structure of the proposed islanding identification scheme.

are resulted in a variations through real-time evaluations. In this case, how much the a_i real-time evaluation varies through small deviations, it is resulted in smaller values for corresponding $MICI_i$ index. To do this, considering a specified threshold near to a_{min} parameter, small $MICI_i$ values are provided.

From Fig. 1, it is seen that by opening circuit breaker SW, the microgrid is operated through islanded operating mode. In this case, the equivalent Thevenin impedance seen from generator terminal Z_G is evaluated as follows:

$$Z_G = Z_L^{eq} + jX_{Tr} \qquad (20)$$

Similarly, in this case, microgrid can be equaled within Thevenin equivalent circuit with a SSG voltage source E_G and equaled impedance Z_G where the proposed online indexes can be implemented though the simplified system without any additional adjustments.

Detailed structure of the proposed real-time scheme developed through different conditional constraint is illustrated in Fig. 4.

From Fig. 4, real-time structure of the proposed islanding scheme consists of four different subsection as follows:

- **Step 1:** At each time window, based on the SSG-based measuring signals, the system frequency $\Delta\omega_{TH}$ and corresponding deviations with respect to time domain evaluations $D\omega_{TH}$ are provided. In this step, similar to

provided passive-based methods, the microgrid voltage and frequency variations are evaluated [23-24].
- **Step 2:** In the case of evaluating $\Delta\omega_{TH}$ and $D\omega_{TH}$ larger than specified threshold criteria, the proposed identification scheme is activated from which based on the metric developed in (18), the proposed *MICI* index is calculated.
- **Step 3:** Depending on the system load level and coefficient factor a, different values of $MICI_i$ are provided which based on the (19), the $MICI_{min}$ is identified. In this case, based on the phasor measurement-based devices installed at generator terminal buses, a set of phasor signals are used which are resulted in less noisy signals through final index evaluations.
- **Step 4:** Based on the developed time window Δt, if, the $MICI_{min}$ index is evaluated lower than predefined value $MICI_0$ (i.e. $MICI_{min} < MICI_0$), an islanding operating mode is identified from which proper protecting decisions are estimated.

3. REQUIRED CONSTRAINTS THROUGH PROPOSED ONLINE INDEX

In this section, based on the concepts of islanding operating scenarios and fault event conditions (FEC), a set of online thresholds are provided which are validated within mathematical formulations. To do this, based on the nature of IOM and FEC, a set of constraints are developed and presented individually through following parts.

3.1. MICI Threshold Adjustments

In the case of dynamic load models, the corresponding coefficient a varies through real-time evaluations. In this case, when the microgrid is disconnected from upstream network and operated within islanded mode, considering dynamic variations of parameters a, it maybe resulted in nonzero values for the proposed *MICI* index (18) through islanded operating mode. Also, in the case of deviating microgrid frequency with respect to fault event scenarios, it will be influenced through equivalent Thevenin resistance seen form load buses R_L [17], which should be considered through *MICI* constraints. In this case, the corresponding load model depended on the microgrid frequency and voltage can be written as follows:

$$P_L = P_0 \left(\frac{V_{LF}}{V_0}\right)^a \times [1 + k_f (\omega(t) - \omega_0)] \qquad (21)$$

Where, the coefficient k_f represents the load type dependency on the microgrid frequency which is varied in the range of 0 to 4 values with respect to load diversities [17]. Also, $\omega(t)$ and ω_0 are the real-time and base frequencies through microgrid system, respectively.

From (21), the total load resistance R_L dependence on the microgrid voltage and frequency parameters can be written as follows:

$$R_L = \left(\frac{V_0^2}{P_0}\right) \times \frac{(V_0/V_{LF})^{a-2}}{[1 + k_f (\omega(t) - \omega_0)]} \qquad (22)$$

Through islanding operating modes, the equivalent load resistance R_L is equaled to microgrid Thevenin resistance R_G. In this case, by substituting (22) in (18), the corresponding *MICI* index modified through both voltage and frequency parameters is rewritten as follows:

$$MICI_i = \left(\frac{(V_0)^{2-a_i}}{R_0} \right) \times$$
$$\left| \left(\frac{d\left(\left(\frac{V_0{}^2}{P_0} \right) \times \frac{(V_0/V_{LF})^{a_i-2}}{[1+k_f(\omega(t)-\omega_0)]} \times \left((V_{LF})^{2-a_i} \right)^{-1} \right)}{d\omega} \right) \right| \quad (23)$$

In the case of small deviations Δa through load dependency coefficient a_i, the proposed *MICI* (23) can be written as:

$$MICI_i = \left(\frac{(V_0)^{2-a_i}}{R_0} \right) \times$$
$$\left| \left(\frac{d\left(\left(\frac{V_0{}^2}{P_0} \right) \times \frac{(V_0/V_{LF})^{a_i+\Delta a-2}}{[1+k_f(\omega(t)-\omega_0)]} \times \left((V_{LF})^{2-a_i} \right)^{-1} \right)}{d\omega} \right) \right| \quad (24)$$

From (24), considering some simplification, the *MICI* index can be represented as follows:

$$MICI_i = \left(\frac{(V_0{}^2/P_0)(V_0)^{\Delta a}}{R_0} \right)$$
$$\times \left| \left(\frac{d}{d\omega} \left(\frac{(V_{LF})^{-\Delta a}}{[1 + k_f(\omega(t) - \omega_0)]} \right) \right) \right| \quad (25)$$

Equation (25) can be written as follows:

$$MICI_i = \left(\frac{(V_0{}^2/P_0)(V_0)^{\Delta a}}{R_0} \right) \times$$
$$\left| \begin{array}{c} \left(\frac{1}{[1+k_f(\omega(t)-\omega_0)]} \frac{d(V_{LF})^{-\Delta a}}{d\omega} \right) + \\ \left((V_{LF})^{-\Delta a} \frac{d}{d\omega} \left(\frac{1}{[1+k_f(\omega(t)-\omega_0)]} \right) \right) \end{array} \right| \quad (26)$$

From Taylor series, it can be derived that

$$\frac{d}{d\omega} \left(\frac{1}{[1 + k_f(\omega(t) - \omega_0)]} \right) \cong \frac{d}{d\omega} (1 - k_f(\omega(t) - \omega_0)) \cong -k_f \quad (27)$$

Therefore, substituting (27) into (26), it is revealed that

$$MICI_i = \left(\frac{(V_0{}^2/P_0)(V_0)^{\Delta a}}{R_0} \right) \times$$
$$\left| \left(-\frac{\left(\Delta a \times V_{LF}^{-(\Delta a+1)} \right)}{[1 + k_f(\omega(t) - \omega_0)]} \frac{d(V_{LF})}{d\omega} - \left(V_{LF}^{-\Delta a} \times k_f \right) \right) \right| \quad (28)$$

Considering islanding operating mode, the total load resistance R_L is identical to microgrid Thevenin resistance R_G which the term (V_0^2/P_0) in (22) is rewritten as follows:

$$\left(V_0{}^2/P_0 \right) = R_G (V_0/V_{LF})^{2-\Delta a} \times [1 + k_f(\omega(t) - \omega_0)] \quad (29)$$

Therefore, the final *MICI* index considering islanding operating mode can be concluded as follows:

$$MICI_i = \frac{R_G}{R_0} (V_{LF})^{a_i+\Delta a-2} (V_0)^{2-a_i} \times \left| \left(-\left(\Delta a \times V_{LF}^{-(\Delta a+1)} \right) \right. \right.$$
$$\left. \left. \frac{d(V_{LF})}{d\omega} - \left(V_{LF}^{-\Delta a} \times k_f \times [1 + k_f(\omega(t) - \omega_0)] \right) \right) \right| \quad (30)$$

From (30), considering different coefficient values between minimum $a_{\min}$ and maximum $a_{\max}$ margins, the $MICI_i$ index is evaluated from which the lowest index $MICI_{\min}$ and corresponding coefficient factor $a_{\min}$ are identified and considered as the candidate thresholds.

In the case of large values of k_f, there are high dependency between the microgird frequency and load model which present sensitive situations for operating the microgrid on islanding mode. However, in the case of small value, loads are independent from the system frequency which can be operated on islanding working mode.

It is worth noting that load coefficient a is highly dependent on the dynamic load model from which estimating the actual value is impossible. In this case, considering the most severe case, the deviation value Δa can be estimated as follows:

$$|\Delta a_{\max}| = \frac{1}{2n} (a_{\max} - a_{\min}) \quad (31)$$

From (31), by identifying the worse cases with respect to both negative $-\Delta a_{\max}$ and positive $+\Delta a_{\max}$ values, the proposed $MICI_i$ indexes are evaluated form which the maximum threshold is estimated as follows:

$$MICI_{TH} = \max \left\{ MICI_{|\Delta a_{\max}|}, MICI_{-|\Delta a_{\max}|} \right\} \quad (32)$$

At each time window, the proposed *MICI* index is evaluated from which the minimum value $MICI_{\min}$ and corresponding $MICI_{TH}$ are identified. Once, the estimated index $MICI_{\min} < MICI_{TH}$, it means an islanding operating scenario is identified from which the corresponding proper protecting strategies are performed. In other cases (i.e. $MICI_{\min} > MICI_{TH}$), there are some fault event conditions estimated by proposed scheme which any IOM-based protective schemes are not estimated through real-time operating conditions. It is worth noting that the proposed threshold (32) is an online index which is adapted continuously with respect to microgrid operating mode. By this way, the most probable islanding scenarios with proper accuracy ratios are estimated. Also, it should be noting that, in the case of islanded operating mode equipped with other types of constant impedance load models as inductance loads paralleled with resistance loads, the proposed *MICI* index provides some tiny nonzero values which should be considered through estimation procedure for proper IOM identification. However, real-time analytical simulations indicate that in the case of IOM scenarios, the evaluated $MICI_{\min}$ index is much lower than provided threshold $MICI_{TH}$ which therefore, it can be well used through microgrid system to accurate estimation of IOM scenarios.

3.2. Fault Event Threshold Adjustments

In the case of IOM, following swing equation, the microgrid frequency deviation is computed as follows [13]:

$$(2H/\omega_0) \frac{d\Delta\omega}{dt} = \Delta P_m - \Delta P_e - (D \times \Delta\omega) \quad (33)$$

Where, ΔP_m and ΔP_e are the microgrid active powers exchanged from installed synchronous generators to

upstream network in the case of before and after IOM, respectively. Also, H and D represent the inertia and damping coefficient provided from synchronous generators, respectively.

By converting (33) through Laplacian transform, the system eigenvalues are calculated as follows [13]:

$$\frac{2H}{\omega_0} S + D = 0 \qquad (34)$$

In the case of first order transfer function, the microgrid time-domain frequency deviation presents an exponential manner within special time constant as follows [13]:

$$\Delta\omega(t) = \frac{1}{D}(\Delta P_M - \Delta P_e) \times \left(1 - e^{-\left(\frac{D \times \omega_0}{2H}\right)t}\right) \qquad (35)$$

From (35), in the case of islanding fault event scenario, the corresponding threshold for microgird frequency deviation $\Delta\omega_{TH}$ during time instance T_S is provided as follows [13]:

$$\Delta\omega_{TH} = \frac{1}{D}(\Delta P_M - \Delta P_e) \times \left(1 - e^{-\left(\frac{D \times \omega_0}{2H}\right)T_S}\right) \qquad (36)$$

From (35) and (36), considering a time-based derivative function, the changing ratio of microgrid frequency deviations is evaluated as follows [13]:

$$\frac{d\Delta\omega}{dt} = \frac{\omega_0}{2H}(\Delta P_M - \Delta P_e) \times e^{-\left(\frac{D \times \omega_0}{2H}\right)t} \qquad (37)$$

From (37), the coefficient $[(D \times \omega_0)/(2H)]$ presents small value into microgrid real cases. Therefore, considering IEEE standard recommended for islanding estimation time (i.e. $t < 2$ second), the exponential function can be approximated as one value from which the corresponding $\Delta\omega_{TH}$ threshold is equaled with following equation [13]:

$$D \times \Delta\omega_{TH} = \frac{d\Delta\omega}{dt} \cong \frac{\omega_0}{2H} \times (\Delta P_M - \Delta P_e) \qquad (38)$$

Based on (38), at each time window, the microgird frequency deviation is measured from which in the case of evaluating $\Delta\omega(t) > \Delta\omega_{TH}$, the corresponding IOM-based protective scheme is provided.

It is worth noting that in the case of large values of H and D, the system dynamic response will be slowed resulted in proper damping performance into the grid. However, in the case of smaller values of H and D, there are fast dynamic oscillations with low damping performances into the system. In this case, considering large values, there are more time for identifying of islanding operation while in the case of smaller values, microgrids experience fast oscillations with lower time on estimating islanding mode.

4. VALIDATION OF PROPOSED SCHEME THROUGH SIMULATION STUDIES

In this section, considering a typical microgrid system, the effectiveness of the proposed islanding protective scheme is investigated. Single line diagram of the microgrid test system equipped with SSG resources and composite load modes is illustrated in Fig. 5. From Fig. 5, by using a CCP circuit breaker, microgrid is connected to upstream

network which is operated through GCOM. It should be noting that all of simulation studies and provided results are carried out through one of the most powerful dynamic stability software DigSILENT$^@$ which dynamic behaviors are investigated through time domain simulations.

In order to evaluate the ability of proposed scheme through IOM and FEC scenarios, a set of simulation case studies are provided which are detailed in Table 1. As it can be seen, there are several types of occurrence scenarios including Type1-Islanding Scenarios (*CS1-CS3*), Type2-Short Circuit faults (*CS4-CS7*), Type3-Motor Starting (*CS8-CS10*) and Type4-Capacitor bank switching scenarios (*CS11-CS13*) which are distributed through different microgrid load flow operating points.

From Table 1, there are different types categorized through *a* and *b* diversity factors. Also, in order to evaluate dynamic load models behaviors, considering a set of induction machines indicated as inertia constant parameter in Table 1, dynamic performance of proposed protective scheme is investigated. In the case of SSGs, each synchronous generator is equipped with one automatic voltage regulator (AVR) and governor from which the system voltage and frequency are controlled.

For evaluating *MICI* index, considering each fault event scenario provided in Table 1, dynamic performance of proposed protective scheme is investigated which the effectiveness is compared with other islanding identification approaches developed in the literatures. In this case, considering different islanding identification techniques as Tech.1 presented in [15], Tech.2 presented in [18], ROCOF method presented in [12] and rate of change of voltage-based method (ROCOV) presented in [15], the accuracy and speed ratios of proposed *MICI* index with provided techniques is compared. The required threshold adjustments related to each provided technique are illustrated in Table 2.

From Table 2, it is seen that presented methods have different thresholds which must be considered individually through each fault event scenario. Also, through proposed MICI scheme, there are different parameters which must be determined. The required parameter adjustments consisting of SSG parameters and corresponding *MICI* index thresholds are presented in Table 3.

From Table 3, the required adjustments are categorized through three different categories as SSG parameters from developed model (33), *MICI* threshold adjustments developed in (36) and (38) and proposed *MICI* index parameters developed in (30). In the case of *MICI* coefficient *a*, considering different values through 0-2 in the steps of 0.25, the *MICI* index value is evaluated. Also, considering proposed flowchart in Fig. 4, by using developed time delay $\Delta t = 30$ ms, the corresponding counter for providing threshold values is equaled to $C_{TH} = 150$ which is evaluated through specified sampling frequency $f_S = 6$ kHz. Also, from Table 3 it is revealed that in the case of based load level through microgrid load flow studies, the *MICI* thresholds are specified as $MICI_{TH} = 3$ and $MICI_{min} = 800$ which are identical as provided description in the last paragraph of Section 3.1.
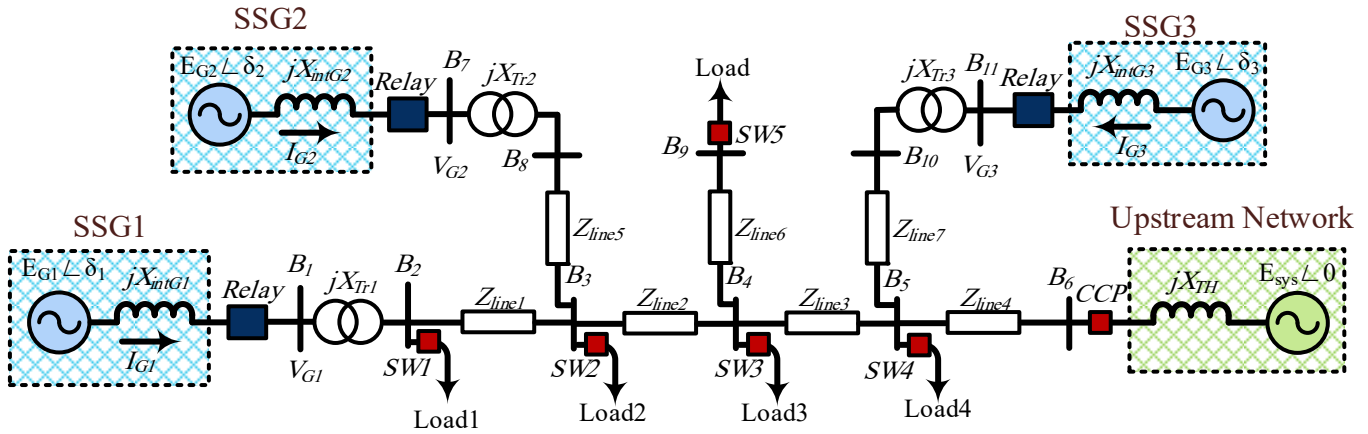
Fig. 5. Single line diagram of the microgrid tests system equipped with SSG and composite load models.

Table 1. Different fault events evaluated through simulation studies

Case Study (CS)		Static Loads Model Parameters				Load Flow Imbalances	Fault Scenario	Dynamic Load Parameter
		Total P (MW)	Total Q (Mvar)	a	b	(ΔP) (%)		
CS1	Islanding Scenarios	9.5	4.5	2	2.5	2	Tripping CPP	Deactivate
CS2		5.5	2.5	1.5	1.75	20	Tripping CPP	H=2.5 s
CS3		6.5	3.5	1	1.25	20	Tripping CPP	H=1.5 s
CS4	Short Circuit	7.5	4.5	0.75	1	20	Short Circuit at B3	H=1 s
CS5		4.5	1.5	0.5	0.75	20	Short Circuit at B4	H=3.5 s
CS6		5.5	3.5	1.25	1.5	20	Short Circuit at B5	H=0.5 s
CS7		8.5	4.5	2.5	2	20	Short Circuit at B9	H=2 s
CS8	Motor Starting Scenarios	9.5	5.5	3	2.5	20	Motor Starting at B4	H=3 s
CS9		8.3	4.6	2	3	20	Motor Starting at B5	H=0.75 s
CS10		5.6	4.2	1.25	2.25	20	Motor Starting at B9	H=1.5 s
CS11	Capacitor Bank Switching Scenarios	6.6	3.3	2.3	1.3	20	Capacitor Switching SW2	H=2.5 s
CS12		7.5	4.2	1.4	2.3	20	Capacitor Switching SW3	H=0.5 s
CS13		5.6	2.4	1.25	1	20	Capacitor Switching SW5	H=1 s

Table 2. Required adjustments through different techniques in the literature

Techniques \ Thresholds	Tech.1 [15]	Tech.2 [18]	ROCOF [12]	ROCOV [15]
TH1 (df/dt)	40 mHz	–	–	–
TH2 (df/dt)	1.9 Hz	–	–	–
Time Delay	40 ms	–	50 ms	150 ms
$(df/dQ)_{min}$	–	0.8 Hz/Mvar	–	–
$(df/dQ)_{max}$	–	8.5 Hz/Mvar	–	–
$(d\omega/dt)$	–	–	0.05 p.u./s	0.01 p.u./s
(dV/dt)	–	–	–	0.2 p.u./s

Table 3. Required threshold adjustments through different techniques

SSG Parameter		Threshold Adjustments				MICI index parameters				
D (33)(p.u.)	H (33)(s)	$\Delta P_{Islaning}$(kW)	T_S (36)(s)	$\Delta\omega_{TH}$ (36)(p.u.)	$D\times\Delta\omega_{TH}$ (38)(p.u./s)	K_f (30)	a (30)	Δt (ms)	$MICI_{\min}$	$MICI_{TH}$
0.0025	0.55	130	0.5	0.005	0.02	3	0≈2	30	800	3

Based on developed parameters in Table 2 and Table 3 and provided fault event scenarios in Table 1, dynamic performance of proposed islanding identification scheme is evaluated through following case studies (CS).

4.1. Case Studies 1 to 3 (Islanding scenarios)

In this section, considering three CSs 1 to 3 from Table 1 specified in IOM, the CCP circuit breaker is disconnected at $t = 1$ second which dynamic performance of proposed scheme is investigated. In CS 1, regarding CCP disconnection, microgrid experience a load flow imbalance about 1.6% nominal active power of installed synchronous generators. Also, it is considered that only constant impedance load models are operated in case study 1. Regarding low level load flow imbalance (i.e. 1.6% of nominal power), the microgrid frequency is deviated in a small boundary which may not be detected by using conventional ROCOF/ROCOV protective relays. Dynamic behaviors of the microgrid frequency ω(p.u.), its rate of change $d\omega$/dt and proposed MICI thresholds $MICI_{\min}$ and $MICI_{TH}$ are presented in Fig. 6.

From Fig. 6, it is revealed that about 155 ms after islanding fault event scenario, the $MICI_{\min}$ online evaluation reached to 1.1 value which is lower than specified $MICI_{TH} = 3$ criteria provided in Table 3. In this case, considering provided islanding identification role (i.e. $MICI_{\min} < MICI_{TH}$), after about 195 ms, proper identification signal is estimated as shown in Fig. 6(d).

In other case, in CS 2, considering a set of dynamic load models as induction machines through microgrid system, the performance of MICI index is evaluated. Online evaluations of $MICI_{\min}$ and $MICI_{TH}$ are presented in Fig. 7.

From Fig. 7, it can be seen that about 110 ms after islanding scenario, the $MICI_{\min}$ evaluations goes lower than $MICI_{TH}$ criteria which after about 165 ms an islanding operaitng scenario is estimated. Similarly, in CS 3, considering different dynamic load-level, $MICI$ online evaluations are investigated form which after about 143 ms, the proper islanding identification signal is estimated.

4.2. Case Studies 4 to 7 (Short circuit fault scenarios)

In the CSs 4 to 7, considering a set of short circuit fault events through GCOM, the MICI online evaluation are investigated. In this case, with respect to short circuit events, some blocking decisions through $MICI$ output identification signals should be estimated. Regarding CSs 4 to 7, considering four types of short circuit fault events consisting of CS4=3-ph short circuit type 1, CS5=3-ph short circuit type 2, CS6=2-ph short circuit and CS7= single phase short circuit occurred at $t = 1$ second, dynamic performance of proposed MICI index is investigated. Dynamic behaviors
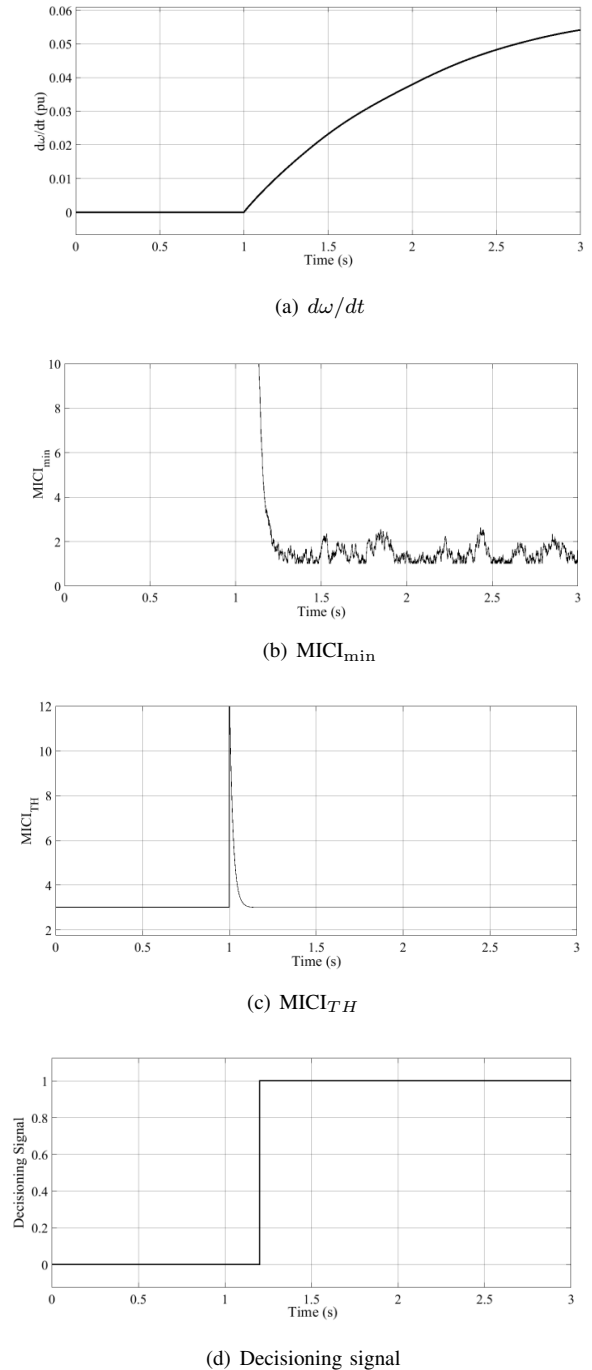

(a) $d\omega/dt$

(b) $MICI_{\min}$

(c) $MICI_{TH}$

(d) Decisioning signal

Fig. 6. *MICI* online evaluation with respect to static load mode in CS1

(a) $d\omega/dt$

(b) $\text{MICI}_{\min}$

(c) MICI_{TH}

(d) Decisioning signal
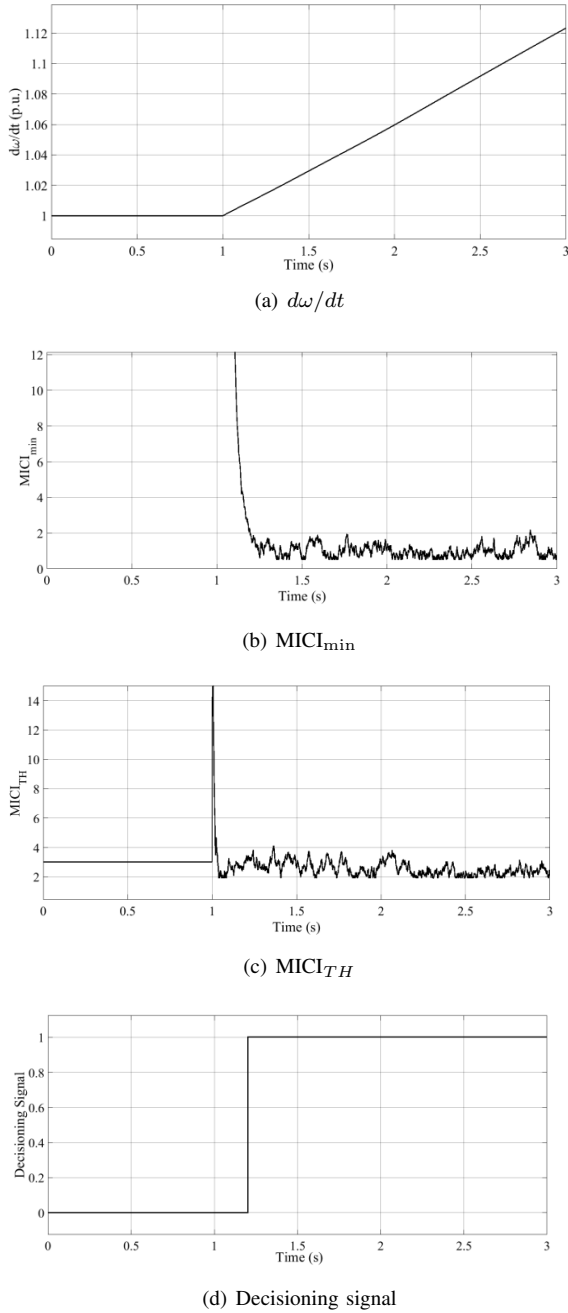
Fig. 7. *MICI* online evaluations with respect to dynamic load mode provided in CS2

(a) $d\omega/dt$

(b) $\text{MICI}_{\min}$

(c) MICI_{TH}

(d) Decisioning signal

Fig. 8. Micrdogrid frequency deviation and corresponding *MICI* estimation with respect to CS4

of the microgrid frequency deviations ω(p.u.), $d\omega/dt$ and corresponding MICI dynamic estimations $MICI_{\min}$ and $MICI_{TH}$ through CS4 are illustrated in Fig. 8.

From Fig. 8, it is concluded that through fault event scenario, the $MICI_{\min}$ are higher than $MICI_{TH}$ criteria which zero value (i.e. blocking signal) is estimated as output decision making signal. Also, in other short circuit cases CS5 to CS7, similar evaluations are processed which the corresponding results are detailed in Table 4.

From Table 4, it is shown that through all of provided short circuit case studies, the proposed *MICI* index works properly which suitable blocking signal are estimated
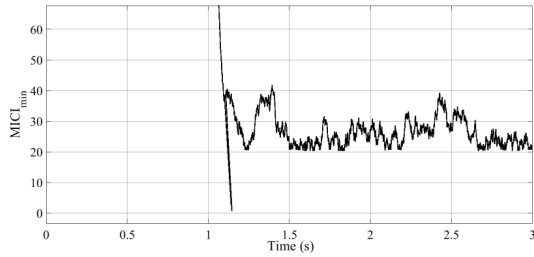
as output decision making signal. It should be noting that through short circuit-based fault events, there are different dynamic behaviors of $MICI_{\min}$ and $MICI_{TH}$ which are deviated through real-time evalution. Fig. 9 presents dynamic evaluation of developed thresholds and corresponding estimating signal through online evaluation of CS6.

Based on Fig. 9(c), it can be seen that through different stable and unstable case studies, there are limited time durations (i.e. lower than 5 ms) which $MICI_{\min}$ goes lower than $MICI_{TH}$ which is much lower than specified time delay $\Delta t = 30$ ms from Table 3 from which the

Table 4. *MICI* estimation results through different short circuit case studies CS4 to CS7
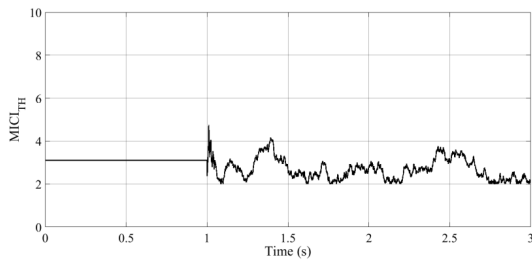
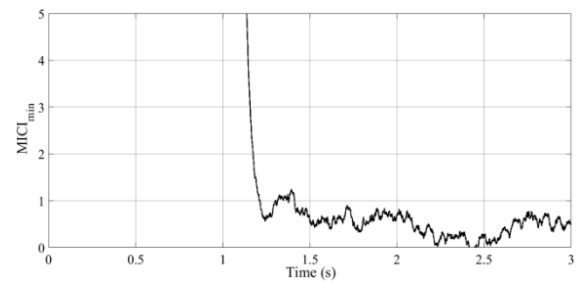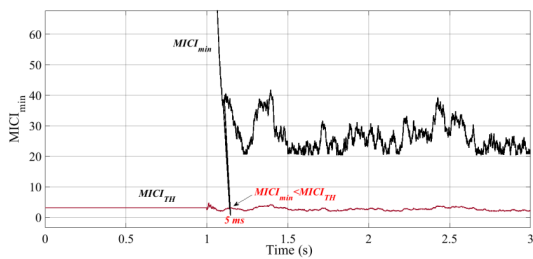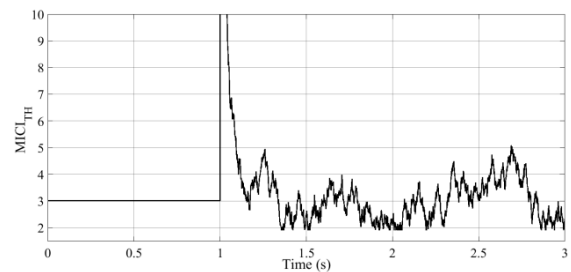| Case Study (CS)	$(\Delta P)(\%)$	Fault	MICI$_{min}$ (Mean Value)	MICI$_{TH}$ (Mean Value)	Islanding Identification Time	Islanding Decision
CS4	20	S.C at B3	40.21	3.75	–	Block
CS5	20	S.C at B4	33.52	3.91	–	Block
CS6	20	S.C at B5	25.34	3.84	–	Block
CS7	20	S.C at B9	21.19	3.63	–	Block

(a) MICI$_{min}$
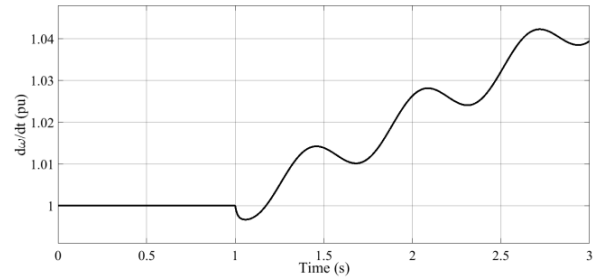
(b) MICI$_{TH}$

(c) Real-time evaluations between the MICI$_{min}$ and MICI$_{TH}$ values.

Fig. 9. Dynamic behaviors of $MICI_{min}$ and $MICI_{TH}$ thresholds through CS6

output decision making signal remains zero value as proper estimation signal. Also, it can be concluded that the proposed protective scheme provide reliable performance with high accuracy ratio through different fault event scenarios which can estimates properly either islanding and fault event scenarios.

4.3. Case Studies 8 to 10 (Motor Starting scenarios)

In this section, considering the motor starting scenarios occurred in different buses, the ability of proposed technique is investigated. In this case, based on the motor inrush

(a) $d\omega/dt$

(b) MICI$_{min}$

(c) MICI$_{TH}$
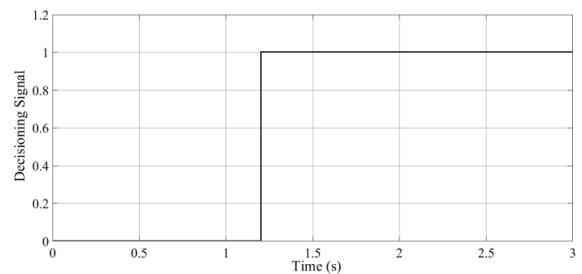
(d) Decisioning signal

Fig. 10. Microgrid frequency deviations and corresponding *MICI* estimations with respect to CS8

current occurred during starting periods, the proposed MICI performance for three CSs 8 to 10 is evaluated. Dynamic behaviors of the microgrid frequency deviations ω and $d\omega/dt$ and corresponding $MICI_{\min}$ and $MICI_{TH}$ performances through CS8 are presented in Fig. 10.

From Fig. 10, considering motor starting at $t = 1\,s$, a large inrush current is occurred which the circuit breaker CCP is tripped after 150 ms. In this case, microgid is islanded from upstream network. Also, it is revealed about 190 ms after motor starting scenario, $MICI_{\min}$ goes lower than $MICI_{TH}$ criteria which islanding operating mode is estimated. Also, in cases CS9 and CS10, similar starting scenarios are developed considering from which, estimation resulted are presented in Table 5.

From Table 5, it is concluded through motor starting scenarios CS9 and CS10, proper islanding estimations are provided which islanding identification signal are estimated as output decision making signal.

4.4. Case Studies 11 to 13 (Capacitor bank switching transients and dynamics)

In this section, reliability of proposed protective scheme against the capacitor bank switching transients are investigated through three different cases as CS 11 to CS13 provided in Table 1. In this case, considering different switching scenarios, performance of proposed *MICI* index is evaluated. Dynamic *MICI* estimations with respect to transient case studies CS11 and CS13 are illustrated in Table 6.

Based on evaluated results from Table 6, it is concluded that the proposed scheme provides reliable behaviors against two important issues as capacitor bank switching transients and dynamics which no mal-operation performances are identified through real-time evaluations.

4.5. Evaluating proposed index with respect to NDZ regions

In this section, the real-time performance of proposed *MICI* index with respect to microgrid NDZ regions is investigated. As described previously in Section 1, NDZs are some special regions through microgird unbalance load flow conditions which are not seen by conventional frequency relays ROCOF and leaded to relay's mal-operations within unbalance situations [25-26]. For this issue, considering microgrid SLD shown in Fig. 1, 175 different load flow imbalances are provided from which *MICI* dynamic performance is evaluated. Estimated islanding scenarios through various identification times with respect to different load flow imbalances are provided in Fig. 11.

From Fig. 11, it is revealed that in the case of load flow imbalances through both active and reactive powers, the corresponding islanding scenarios are estimated lower than 2 seconds which can be represented as a considerable result through proposed protective scheme evaluations. However, in the case of zero power imbalances, similar to presented passive techniques, the proposed scheme involves with some unwanted mal-operations through proper identification cases.
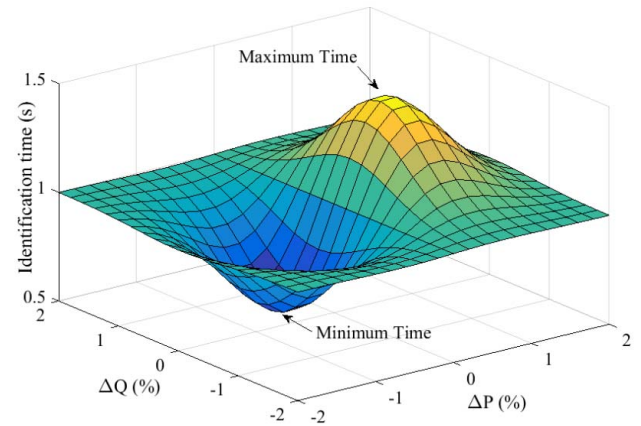

Fig. 11. MICI estimations with respect to different load flow imbalances

4.6. Comparing the proposed scheme with respect to other passive approaches

From Table 2, there are some passive techniques which have been introduced for comparing the proposed scheme through different fault event conditions. In this case, considering similar evaluations presented in Section 4.1 to Section 4.4, dynamic performance of developed techniques are evaluated. Comparison results proposed *MICI* scheme with respect to developed passive techniques are illustrated in Table 7.

From Table 7 it can be concluded that the proposed protective scheme presents faster and more accurate estimations with respect to other developed techniques which lower than 200 ms (i.e. it is much lower than IEEE standard identification time 2 seconds) after fault events scenarios, islanding operating scenarios are estimated. Also, in the case of non-islanding scenarios, the proposed scheme works properly without any mal-operation through real-time performance. However, evaluating other passive techniques revealed that they have involved through some improper actions under different fault event scenarios and load flow imbalance conditions.

Based on the developed evaluations, the proposed *MICI* index presents reliable and accurate results for online identification of microgrid islanding scenarios, and therefore can be used as a proper protective scheme through microgrid real-time evaluations.

5. FURTHER DISCUSSIONS

The case studies developed in Sections 4.1 to Section 4.4 present the effectiveness of the proposed scheme for online detection of islanding cases over different microgrid operating conditions. In this section, based on developed investigations, the main merits and possible shortcomings of the proposed approach are presented.

The proposed scheme resolves the issue that the islanding detection might remarkably vary when the classic fixed detection techniques fails, so, in the proposed scheme, sustainable operation of the microgrid for long-term studies can be warranted. In another view, based on the required

Table 5. *MICI* estimation results through islanded short circuit case studies CS9 and CS10

Case Study (CS)	$(\Delta P)(\%)$	Motor Starting	MICI$_{\min}$ (Mean Value)	MICI$_{TH}$ (Mean Value)	Islanding Identification Time	Islanding Decision
CS9	20	at B5	1.34	3.23	143 ms	Estimated
CS10	20	at B9	1.67	3.65	112 ms	Estimated

Table 6. *MICI* estimation with respect to switching transient and motor starting

Case Study (CS)	Fault	$MICI_{\min}$ (Mean Value)	$MICI_{TH}$ (Mean Value)	Islanding Identification Time	Islanding Decision
CS11	Cap. Switching at SW2	41.23	2.89	–	Block
CS12	Cap. Switching at SW3	36.57	3.19	–	Block
CS13	Cap. Switching at SW5	31.14	3.79	–	Block

Table 7. Comparing proposed *MICI* results with respect to other passive techniques

Case Study (CS)	Tech.1 [15]		Tech.2 [18]		ROCOF [12]		ROCOV [15]		Proposed MICI	
	Identification Time (ms)	Islanding Decision	Identification Time (ms)	Islanding Decision	Identification Time (ms)	Islanding Decision	Identification Time (ms)	Islanding Decision	Identification Time (ms)	Islanding Decision
CS1	305	Est.	231	Est.	365	Est.	327	Est.	195 ms	Est.
CS2	215	Est.	198	Est.	305	Est.	295	Est.	165 ms	Est.
CS3	209	Est.	196	Est.	402	Est.	261	Est.	143 ms	Est.
CS4	–	Block	210	Failed	296	Failed	–	Block	–	Block
CS5	–	Block	225	Failed	295	Failed	–	Block	–	Block
CS6	–	Block	–	Block	–	Block	235	Failed	–	Block
CS7	–	Block	–	Block	–	Block	242	Failed	–	Block
CS8	255	Est.	166	Failed	165	Failed	–	Failed	190 ms	Est.
CS9	211	Est.	198	Est.	321	Est.	246	Failed	143 ms	Est.
CS10	202	Est	291	Est	–	Failed	245	Failed	112 ms	Est
CS11	–	Block	–	Block	–	Block	–	Block	–	Block
CS12	–	Block	–	Block	–	Block	412	Failed	–	Block
CS13	–	Block	–	Block	–	Block	263	Failed	–	Block

computation time, the proposed scheme prevents system frequent performances leaded to continuously tracking of the microgrid security, which might result in increasing the risk of microgrid dynamic transient situation, so that it can also warranty stable operation of proposed approach in short-term duration. Above all, the proposed approach is proper for the specific situation in which the fault scenarios keep stable in a short period but varies highly in a long period.

However, through computation procedure of the proposed scheme, some adjustments also need to be defined offline, and then put them in online working mode. In the case of changing the microgrid impedance matrix more frequently, accordingly, the proposed technique needs to be updated more frequently, which might lead improper actions. Another case will be happened when the proposed scheme loses its effectiveness when the online signal transmitted within delay which remarkably effects on method performance. It means that in the case of delay on online signals, the proposed scheme cannot compensate the delay and may

even failed on estimating islanding detection time. In this case, the method should be taken out of service.

For future studies, one of valuable suggestion for developing the proposed schemes can be found through evaluating the proposed controlling scheme on experimental test systems consisting of real values. To do this, considering the proposed controlling structure modeled on laboratory microgrid small scale test system, effectiveness of the proposed islanding scheme can be evaluated. Also, evaluating the proposed approach on large-scale multi-microgrid systems is an interesting topic which can evaluated on future studies.

6. CONCLUSIONS

In this paper, based on the concept of Thevenin impedance evaluated from generator terminals, an adaptive islanding detection scheme has been developed. For this issue, considering microgrid system equipped with SSG resources and complex load models dependence on the system voltage and frequency, the system equivalent Thevenin circuit is

Appendix 1: SSSG dynamic parameters

Parameter (Unit)	Description	Value		
		SSG1	SSG2	SSG3
X_d [p.u.]	D-Axis steady state reactance	1.85	0.66	1.71
X'_d [p.u.]	D-Axis transient reactance	0.268	0.301	0.271
X''_d [p.u.]	D-Axis sub-transient reactance	0.179	0182	0190
X_q [p.u.]	Q-Axis steady state reactance	1.012	1.11	1.74
X''_q [p.u.]	Q-Axis sub-transient reactance	0.193	0.184	0.301
X_p [p.u.]	Reactance at nominal load	0.177	0.181	0.172
R_a [p.u.]	Stator dc resistance	0.006	0.005	0.004
T'_{do} [s]	Open circuit transient time constant	4.15	3.85	1.35
T'_d [s]	Short circuit transient time constant	0.631	0.524	0.211
T''_{do} [s]	D-Axis open circuit sub-transient time constant	0.051	0.04	0.022
T''_d [s]	D-Axis short circuit sub-transient time constant	0.033	0.055	0.015
T''_{qo} [s]	Q-Axis open circuit sub-transient time constant	0.251	0.06	0.11
T''_q [s]	Q-Axis short circuit sub-transient time constant	0.049	0.031	0.018
H [s]	Inertia constant	0.61	0.92	0.66

developed. Then, based on evaluating equivalent Thevenin resistance validated through mathematical formulations, the proposed online *MICI* index is provided. In this case, at each time window, considering two provided thresholds $MICI_{\min}$ and $MICI_{TH}$, the microgrid dynamic security and corresponding operating mode are evaluated. In this case, once provided $MICI_{\min}$ estimates lower than $MICI_{TH}$ criteria, means an IOM which corresponding protective signals are estimated.

The proposed scheme is an online and adaptive scheme which provides fast, reliable and accurate performances under different fault event scenarios. For this issue, different scenarios as switching transients and load starting conditions have been investigated. Simulation results revealed that through all of non-islanded fault events, the proposed *MICI* scheme provides proper estimation (i.e. blocking signals) without any mal-operation. Also, for evaluating the microgrid NDZ issues, different load flow imbalances have been developed through microgrid test system which through all of cases, proper islanding detections have been estimated. As a result, the proposed *MICI* index is an adaptive protective scheme which can be used simply through microgrid system with proper protective outcomes.

DATA AVAILABILITY STATEMENT

The used or generated data and the result of this study are available upon request from the corresponding author.

REFERENCES

[1] M. Rezaee, M. S. Moghadam, and S. Ranjbar, "Online estimation of power system separation as controlled islanding scheme in the presence of inter-area oscillations," *Sustainable Energy, Grids and Networks*, vol. 21, p. 100306, 2020.

[2] A. H. Fathi-Jowzdani, I. Sadeghkhani, and A. Mehrizi-Sani, "Islanding detection for dc microgrids based on episode of care severity index," *IEEE Transactions on Smart Grid*, vol. 13, no. 2, pp. 954–961, 2021.

[3] S. Ranjbar, "Statcom-based intelligent wide-area controller for damping interarea oscillation," *IEEE Systems Journal*, 2023.

[4] C. Blanco, F. Paz, I. G. Zurbriggen, P. Garcia, and M. Ordonez, "Distributed islanding detection in multisource dc microgrids: Pilot signal cancelation," *IEEE Access*, vol. 10, pp. 78370–78383, 2022.

[5] S. Ranjbar, "Adaptive criteria of estimating power system separation times based on inter-area signal," *IET Generation, Transmission & Distribution*, vol. 17, no. 3, pp. 573–588, 2023.

[6] A. Sankar, R. Sunitha, *et al.*, "Synchrophasor data driven islanding detection, localization and prediction for microgrid using energy operator," *IEEE Transactions on Power Systems*, vol. 36, no. 5, pp. 4052–4065, 2021.

[7] S. Ranjbar, M. Aghamohammadi, and F. Haghjoo, "A new scheme of wadc for damping inter-area oscillation based on cart technique and thevenine impedance," *International Journal of Electrical Power & Energy Systems*, vol. 94, pp. 339–353, 2018.

[8] M. W. Altaf, M. T. Arif, S. Saha, S. N. Islam, M. E. Haque, and A. M. Oo, "Effective rocof-based islanding detection technique for different types of microgrid," *IEEE Transactions on Industry Applications*, vol. 58, no. 2, pp. 1809–1821, 2022.

[9] A. M. Niaki and S. Afsharnia, "A new passive islanding detection method and its performance evaluation for multi-dg systems," *Electric Power Systems Research*,

vol. 110, pp. 180–187, 2014.

[10] M. Dehghanzade Golmaee, A. Koochaki, and S. Ranjbar, "Variable frequency transformer equipped with dynamic breaking resistors for controlling low frequency oscillation using hierarchical strategy," *Electrical Engineering*, vol. 105, no. 1, pp. 113–128, 2023.

[11] R. Bakhshi-Jafarabadi, J. Sadeh, and M. Popov, "Maximum power point tracking injection method for islanding detection of grid-connected photovoltaic systems in microgrid," *IEEE Transactions on Power Delivery*, vol. 36, no. 1, pp. 168–179, 2020.

[12] S. Ranjbar, "Online estimation of controlled islanding time intervals using dynamic state trajectories through cascading failures from wams data," *Electric Power Systems Research*, vol. 214, p. 108890, 2023.

[13] S. F. Zarei, H. Mokhtari, and F. Blaabjerg, "Fault detection and protection strategy for islanded inverter-based microgrids," *IEEE Journal of Emerging and Selected Topics in Power Electronics*, vol. 9, no. 1, pp. 472–484, 2019.

[14] S. Roudi, R. Ebrahimi, M. Ghanbari, and S. Ranjbar, "Virtual generator-based damping controller for microgrids with low inertia resources based on energy storage systems," *International Transactions on Electrical Energy Systems*, vol. 31, no. 5, p. ete12832, 2021.

[15] I. Sepehrirad, R. Ebrahimi, E. Alibeiki, and S. Ranjbar, "Intelligent differential protection scheme for controlled islanding of microgrids based on decision tree technique," *Journal of Control, Automation and Electrical Systems*, vol. 31, pp. 1233–1250, 2020.

[16] S. Ranjbar, A. S. Al-Sumaiti, R. Sangrody, Y.-J. Byon, and M. Marzband, "Dynamic clustering-based model reduction scheme for damping control of large power systems using series compensators from wide area signals," *International Journal of Electrical Power & Energy Systems*, vol. 131, p. 107082, 2021.

[17] S. Ranjbar, "Online estimation of controlled islanding time intervals using dynamic state trajectories through cascading failures from wams data," *Electric Power Systems Research*, vol. 214, p. 108890, 2023.

[18] S. Mahdavizadeh, M. Aghamohammadi, and S. Ranjbar, "Frequency stability-based controlled islanding scheme based on clustering algorithm and electrical distance using real-time dynamic criteria from wams data," *Sustainable Energy, Grids and Networks*, vol. 30, p. 100560, 2022.

[19] M. Jalilian, A. Rastgou, S. Kharrati, and S. Hosseini-Hemati, "Frequency stability of hybrid power system in the presence of superconducting magnetic energy storage and uncertainties," *Journal of Operation and Automation in Power Engineering*, vol. 11, no. 4, pp. 230–239, 2023.

[20] K. Matharani and H. Jariwala, "Stability analysis of microgrid with passive, active, and dynamic load," *Journal of Operation and Automation in Power Engineering*, vol. 11, no. 4, pp. 295–306, 2023.